

Article

# A Study on the Microstructure and Corrosion Characteristics of Early Iron Age Bronze Mirrors Excavated from the Korean Peninsula

Nam Chul Cho <sup>1,\*</sup>, Min Kyeong Jang <sup>2</sup>  and Il Kwon Huh <sup>3</sup><sup>1</sup> Department of Cultural Heritage Conservation Sciences, Kongju National University, Gongju-si 32588, Korea<sup>2</sup> Collections Management Division, Seoul Baekje Museum, Seoul 05540, Korea; jmink1028@gmail.com<sup>3</sup> Conservation Science Division, National Museum of Korea, Seoul 04383, Korea; kick19@korea.kr

\* Correspondence: nam1611@kongju.ac.kr; Tel.: +82-42-850-8541

**Abstract:** Bronze mirrors, considered important grave goods, were widely used before glass mirrors in ancient times. Most excavated bronze artifacts are covered with corrosive materials and lose their original colors. More importantly, identifying corrosion characteristics and the manufacturing techniques used for these artifacts are essential for proper artifact preservation. In this study, Early Iron Age bronze mirrors excavated from the Korean Peninsula were examined to determine their microstructures, corrosion characteristics, and production techniques using various analytical methods, such as Micro-Raman spectroscopy and field emission electron probe microanalysis. As a result, sulfides containing iron suggested chalcopyrite use during production or that the sulfides originated from copper, iron, and sulfur residual matte. The analysis also detected corrosion layers with high tin oxide (SnO<sub>2</sub>) levels and selective corrosion in the  $\alpha + \delta$  eutectoid phase on the artifact's surface. In the corrosive layer, cuprite, malachite, and cassiterite corrosion products were detected, and nanocrystalline SnO<sub>2</sub> was identified as a characteristic of long-term soil erosion. Identifying these artifacts' corrosion characteristics and manufacturing techniques is essential and can greatly contribute to proper artifact preservation.

**Keywords:** Early Iron Age; bronze mirror; artifact preservation; production techniques; corrosion



**Citation:** Cho, N.C.; Jang, M.K.; Huh, I.K. A Study on the Microstructure and Corrosion Characteristics of Early Iron Age Bronze Mirrors Excavated from the Korean Peninsula. *Appl. Sci.* **2021**, *11*, 2441. <https://doi.org/10.3390/app11052441>

Academic Editor: Emanuela Bosco

Received: 9 February 2021

Accepted: 5 March 2021

Published: 9 March 2021

**Publisher's Note:** MDPI stays neutral with regard to jurisdictional claims in published maps and institutional affiliations.



**Copyright:** © 2021 by the authors. Licensee MDPI, Basel, Switzerland. This article is an open access article distributed under the terms and conditions of the Creative Commons Attribution (CC BY) license (<https://creativecommons.org/licenses/by/4.0/>).

## 1. Introduction

Most currently excavated bronze artifacts are corroded, showing a loss of their original surface colors and being covered with corrosion products. Prolonged burial of bronze artifacts leads to erosion, resulting in morphological changes to stable states and forming various corrosion products. Some representative bronze corrosion products found in ancient bronze artifacts include cuprite (Cu<sub>2</sub>O), tenorite (CuO), malachite (Cu<sub>2</sub>CO<sub>3</sub>(OH)<sub>2</sub>), and paratacamite (Cu<sub>2</sub>Cl(OH)<sub>3</sub>). Here, the corrosion products' type and shape are affected by various factors, such as the artifact's composition, manufacturing technique, size, and burial environment [1]. Furthermore, because of differing conditions, the burial environment can be inferred based on the corrosion products. However, unlike artificial corrosion tests, the corrosion characteristics of naturally corroded bronze artifacts do not appear uniformly. Therefore, data on corrosion characteristics obtained from relics with known excavation sites can play a crucial role in artifact authenticity, preservation, and long-term corrosion research.

The Wanju Sinpung ruins and tomb complex (dated approximately 300 to 200 BCE), excavated from 2010 to 2011, is a site representative of Korea's early Iron Age that shows the transition and social development of tombs. As a result, weapons (bronze swords and arrowheads), tools (chisels and burin), and various bronze artifacts (bronze mirrors) were discovered [2]. Specifically, bronze mirrors describe the temporal and spatial transition of Korean bronzeware, which researchers use to explain the development of bronzeware

manufacturing techniques [3]. In this study, various analytical methods were applied to the bronze mirrors excavated from the Wanju Sinpung ruins to investigate their microstructures, corrosion characteristics, and manufacturing processes.

## 2. Materials and Methods

### 2.1. Materials

The first bronze mirror (Ga-2) was excavated on the bedrock at the site's center, with the mirror side facing upward. From the brim to the upper handle, only a part of the artifact remained, and its surface had a relatively regular corrosion layer. A second mirror (Ga-31) was found in scattered pieces, and its surface had a regular layer of black corrosion. Meanwhile, a third mirror (Ga-35) was found erect in the pit's left-hand side, with the mirror side facing toward the tomb's center. However, two knobs were partially lost. The left-hand knob had traces of a mold mounted for boring holes during the molding process; the presence of fine patterns indicated that it was used for ceremonial purposes (Figure 1) [4].

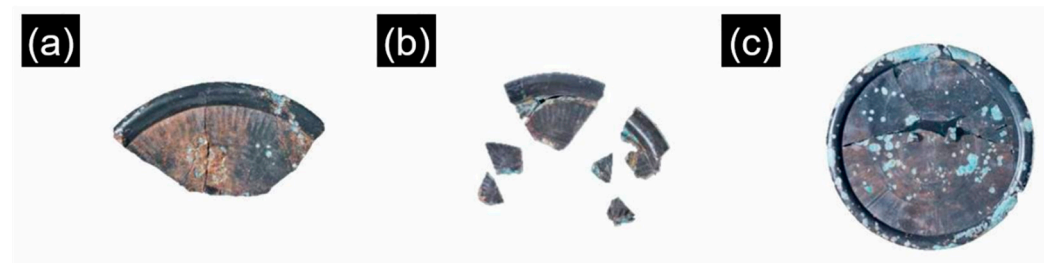


**Figure 1.** Bronze mirrors from the Sinpung Site in Wanju labeled (a) Ga-2, (b) Ga-31, and (c) Ga-35.

### 2.2. Metallography

Samples were obtained from areas already damaged during excavation, areas that lacked patterns, or areas that could not be restored. The samples were mounted with an epoxy resin for metallographic study and polished using silicon carbide grinding pads (220, 500, 1200, 2000, and 4000 grit) with water- and diamond-water-based suspensions (3 and 1 mm, respectively) on a microcloth pad. The samples were etched with a 3% ferric chloride ( $\text{FeCl}_3 + \text{HCl} + \text{ethyl alcohol}$ ) solution for 2 to 3 s during the final step. Meanwhile, the microstructural observation was performed using a metallurgical microscope (Leica, DM4 M). A brightfield (BF) setting was used to observe the microstructure and secondary copper, while surface corrosion compounds were observed using the darkfield (DF) setting.

### 2.3. Inductively Coupled Plasma Atomic Emission Spectroscopy Analysis

Inductively coupled plasma atomic emission spectroscopy (ICP-AES; Perkin Elmer, Optima 4300 DV) was used for composition analysis. The samples were initially placed in a 25 mL conical flask and dissolved with 2 mL of aqua regia while heated on a heating plate. After the samples were gradually dissolved at room temperature and complete dissolution was verified, the solution was transferred to a volumetric flask to obtain 50 g of dissolved sample. The solution was then diluted with a 1000 ppm BDH Spectrosol solution, and 1 mL of aqua regia was added to match a sample matrix. The results were quantified by obtaining the average value of three analyses for various elements, namely copper (Cu), tin (Sn), lead (Pb), arsenic (As), silver (Ag), cobalt (Co), iron (Fe), nickel (Ni), antimony (Sb), and zinc (Zn).

### 2.4. SEM and EDS Analysis

A scanning electron microscope (SEM; TESCAN, MIRA LMH) and an energy dispersive spectrometer (EDS; Perkin Elmer, Waltham, MA, USA, Optima 4300 DV) were used for cross-sectional observation. The samples were coated in platinum (Pt) to enhance their surface conductivity before being subjected to backscattered electron image (BSEI) analysis to obtain clearer, contrasting images.

### 2.5. Field Emission Electron Probe Microanalysis

Field emission electron probe microanalyzer (EPMA) analysis (JEOL Ltd., Akishima, Japan, JXA-8530F) was used to map the images' cross-sections. Once completed, line analysis was used to identify the elemental distribution differences at each level.

### 2.6. Micro-Raman Spectroscopic Analysis

Micro-Raman spectroscopic analysis (Horiba Jobin Yvon, Edison, NJ, USA, LabRAM Aramis) was used to identify corrosion products on the bronze mirrors, and identification was performed using Raman reference values [5]. For Raman analysis conditions, the following settings were used: grid (600 gr/mm), resolution ( $3.0\text{ cm}^{-1}$ ), laser power (1 mW), and acquisition time (60 s). An argon-ion laser, set to 514 nm (wavelength), was used during this step.

## 3. Results and Discussion

### 3.1. Bronze Mirror Excavated from Pit Tomb Ga-2 (No. 1)

#### 3.1.1. Metal

The mirror's microstructure consisted of an  $\delta$  phase, containing fine lines and nodular particles, and an  $\alpha + \delta$  eutectoid phase between the  $\delta$  phase's spaces. Here, the  $\delta$  phase, found in the  $\gamma$  phase's boundary lines, was created during early microstructure formation or in circular patterns around the Pb particles [6]. The microstructure's presence suggested that the mirror was cast using molten metal with an even chemical composition, and no additional treatments were performed after casting (Figures 2a and 3a). Furthermore, the microstructure contains sporadic amounts of sulfides and Pb (Table 1).

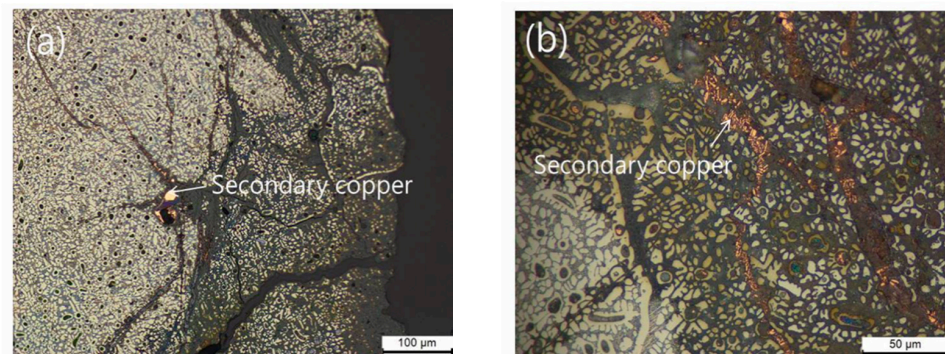


**Figure 2.** (a) Ga-2 (No. 1) optical micrograph showing secondary copper formed in cracks and (b) secondary copper formed in the corroded ( $\alpha + \delta$ ) phase.

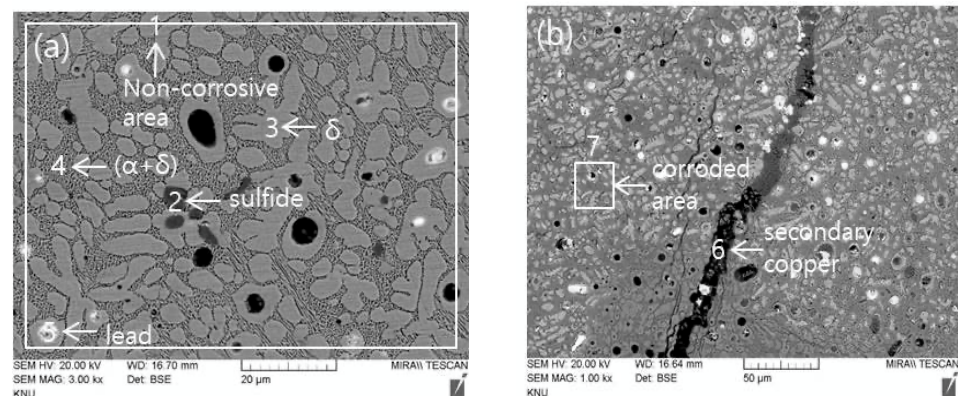


**Figure 3.** Ga-2 (No. 1) scanning electron microscope-energy dispersive spectrometer (SEM-EDS) image. (a) Original microstructure without corrosion and (b) secondary copper grains in corroded microstructures and cracks.

**Table 1.** Ga-2 (No. 1) microstructure energy dispersive spectrometer (EDS) results.

No.	Position	Element (wt%)						
		O	S	Cu	Sn	Pb	Fe	Cl
1	1	0.83	—	69.58	28.02	1.57	—	—
	2	—	21.97	74.71	—	3.32	—	—
	3	0.42	—	65.98	33.60	—	—	—
	4	—	—	73.15	26.85	—	—	—
	5	—	—	67.54	30.36	2.10	—	—
	6	—	1.41	86.89	2.84	5.78	0.65	2.44
	7	11.35	—	33.07	51.34	3.44	—	0.81

Secondary copper is a highly pure metallic Cu formed within a bronze artifact's microstructure. These are mostly formed between layers of corrosion materials, particularly in fractures created by external forces, defects in the casting process, holes created by corroded Pb particles, or  $\alpha + \delta$  eutectoid sites lost through corrosion. Multiple processes, such as electrolysis, generation of residual Cu particles, and rapid changes in the burial environment, can explain secondary copper formation [7]. Here, secondary copper observed in the Ga-2 bronze artifact were small particles found in cracks (Figures 2b and 3b). These are common features found in ancient bronze artifacts, which can be observed when the artifacts corrode over extended periods [8].

### 3.1.2. Patina

Enlarging the corrosion layers of the bronze mirror in DF photography revealed thick, localized layers of red and green corrosion products (Figure 4a). Alternating layers of corrosion material indicated an irregular series of changes in the burial environment. According to the bronze artifact corrosion layer classification system proposed by Robbiola et al. [9], this mirror's corrosion was classified under the type II corrosion category; type II corrosion is identified when corrosion products, such as malachite and cuprite, are present. Micro-Raman spectroscopy was then used to identify these corrosion products. Here, red corrosion products (a) were identified as cuprite ( $\text{Cu}_2\text{O}$ ), dark green corrosion products (c) were malachite ( $(\text{Cu}_2\text{CO}_3(\text{OH})_2)$ ), and bright green corrosion product (b and d) were cassiterite ( $\text{SnO}_2$ ). Notably, cassiterite is the mineral form of  $\text{SnO}_2$ , and the Raman shift observed in the bronze mirror had significant differences from the reference value (Figure 4b) [5]. In this study, the major Raman shift of cassiterite was moderately observed at a range of  $545 \text{ cm}^{-1}$  to  $568 \text{ cm}^{-1}$ . Meanwhile, the Raman shift of natural tin oxide cassiterite, the reference, generally shows a Raman shift ranging from  $633 \text{ cm}^{-1}$  to  $775 \text{ cm}^{-1}$  (Figure 4c). Raman researchers reported that in nanocrystalline  $\text{SnO}_2$ , a wide band that appears below  $580 \text{ cm}^{-1}$  was observed (Figure 4c) [10]. Based on existing research, nanocrystalline  $\text{SnO}_2$  Raman shifts were observed at  $486 \text{ cm}^{-1}$ ,  $568 \text{ cm}^{-1}$ , and  $706 \text{ cm}^{-1}$  [11–13]. Therefore, the cassiterite found in the bronze mirror is nanocrystalline  $\text{SnO}_2$ . Since cassiterite is generated during long-term soil burial, the possibility of uniform detection is low, and a Raman shift error occurred. The possibility of substitution due to various environmental changes during soil burial also cannot be excluded. More importantly, the presence of nanocrystalline  $\text{SnO}_2$  can be attributed to long-term bronze corrosion in a burial environment.

EPMA analysis found that Sn content increased significantly toward the edges' corrosion layers, which contained  $\text{SnO}_2$  (Figure 5). Excluding highly reducing environments with low pH,  $\text{SnO}_2$  could be found in a wide zone between the  $\text{PO}_2 = 1$  and  $\text{PH}_2 = 1$  bars in a stable state, as seen in the Cu-Sn-Cl- $\text{H}_2\text{O}$  Eh-pH diagram. Moreover, the Gibbs energies of  $\text{SnO}_2$  and  $\text{Cu}_2\text{O}$  are  $-519 \text{ kJ/mol}^{-1}$  and  $-416 \text{ kJ/mol}^{-1}$ , respectively, at a temperature of  $24.85 \text{ }^\circ\text{C}$ . These findings, along with the insolubility of  $\text{SnO}_2$ , explain the high levels of Sn in the artifact's corrosion layers [7].

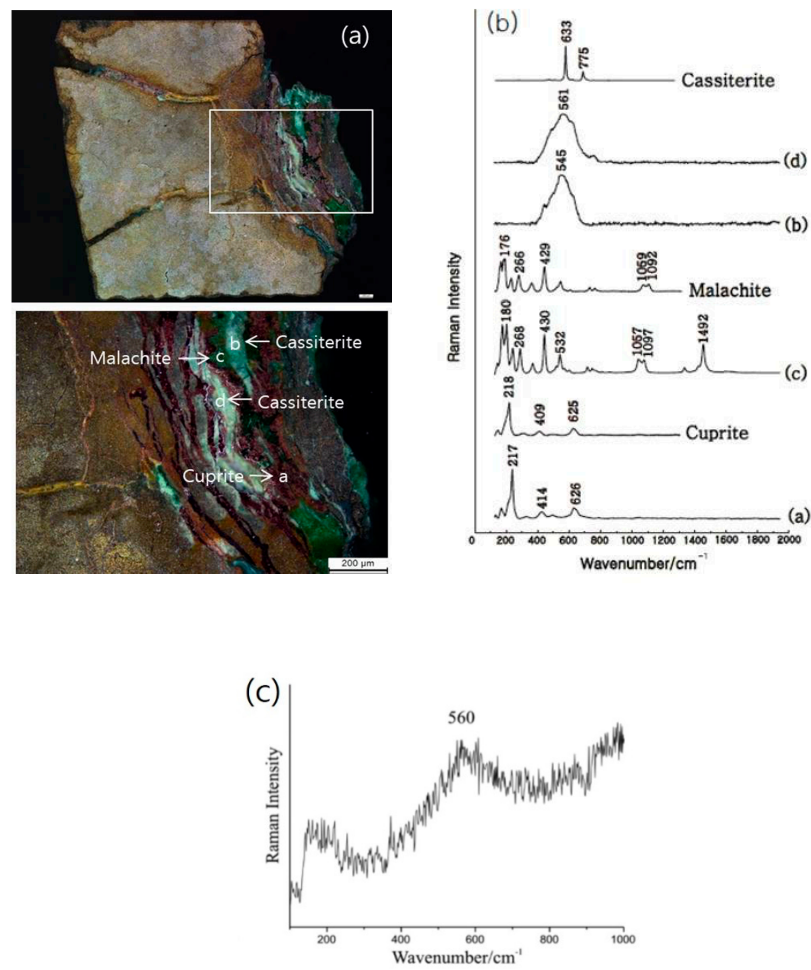


Figure 4. (a) Ga-2 (No. 1) corrosion layer darkfield (DF) images, (b) Raman spectrum, and (c) Raman spectrum of nanocrystalline SnO<sub>2</sub>.

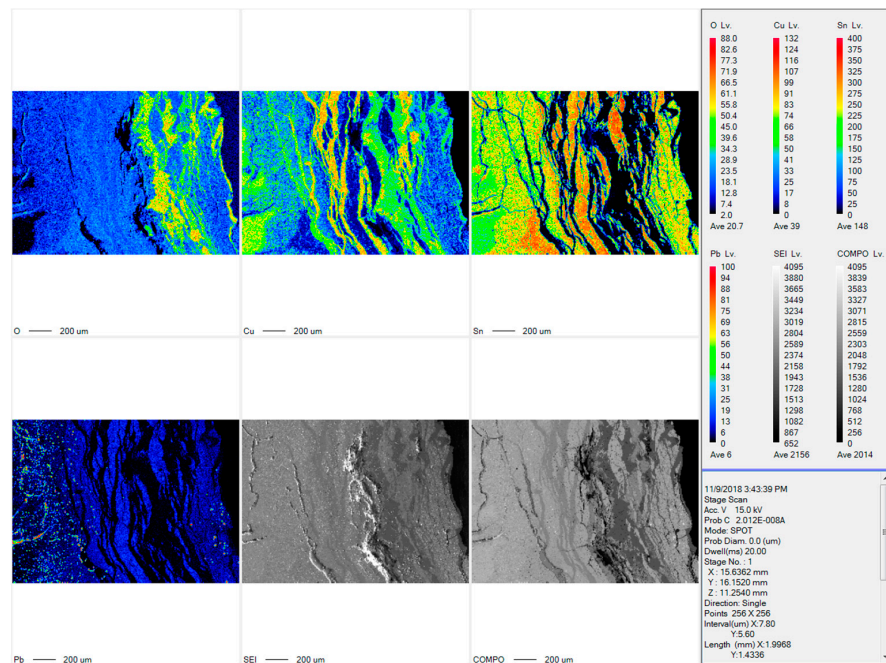


Figure 5. Ga-2 (No. 1) electron probe microanalyzer (EPMA) mapping image.

### 3.2. Bronze Mirror Excavated from Pit Tomb Ga-31 (No. 2) Metal

Given the selective corrosion in the  $\alpha + \delta$  eutectoid phases along the sample's outline and the lack of malachite and cuprite corrosion layers, this mirror's corrosion was classified under type I corrosion [9]. This type of corrosion grows toward the original metallic layer without outward changes in volume and shows high corrosion resistance. Here, this type resulted from generalized corrosion related to the formation of passive layers. Because the  $\alpha + \delta$  eutectoid phase is a combination of two distinct phases, it has a higher electric potential difference compared to the single solid phases at the  $\alpha$  or  $\delta$  phases. Namely, it is a priority target for corrosion because of its structural flaws. Corrosion on the  $\alpha + \delta$  eutectoid phase gradually changed to a dark-blue corrosion product, which is unclear and occluded under microscopic examination and etched during the macroscopic examination. EDS and EPMA mapping analyses revealed that severe corrosion lowered its Cu content and increased oxygen (O) and Sn levels, indicating partial tin oxide mineralization (Figure 6). This oxide formed cryptocrystalline cassiterite structures ( $\text{SnO}_2$ ) and created unclear boundaries [14].

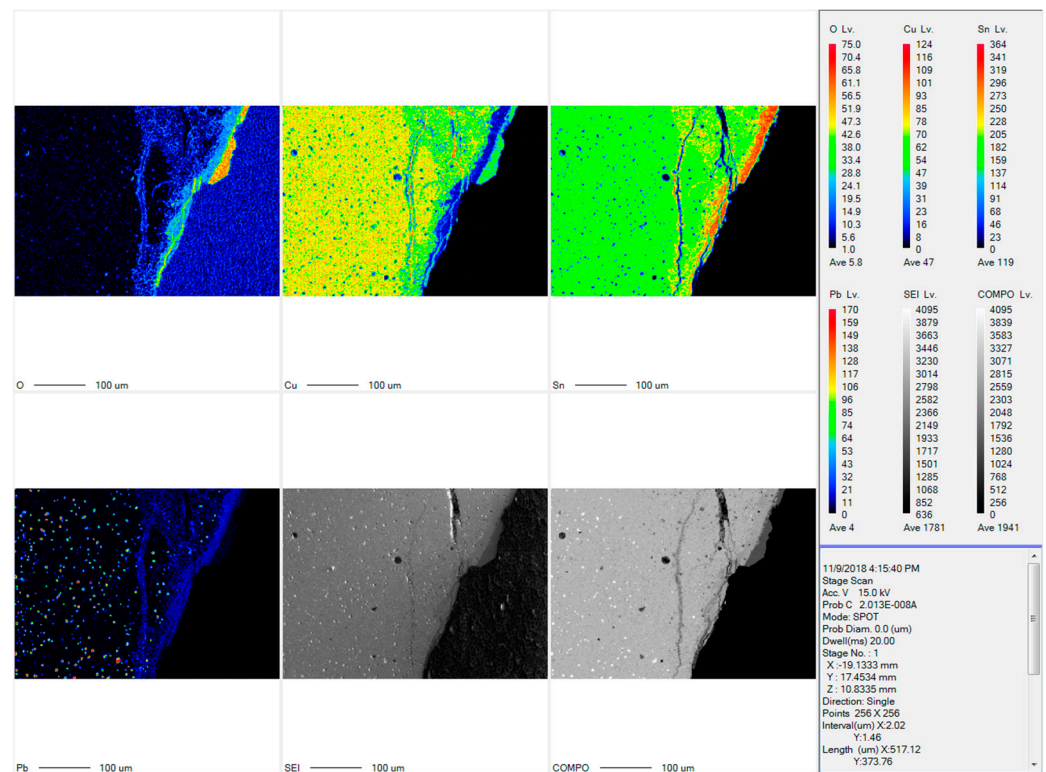
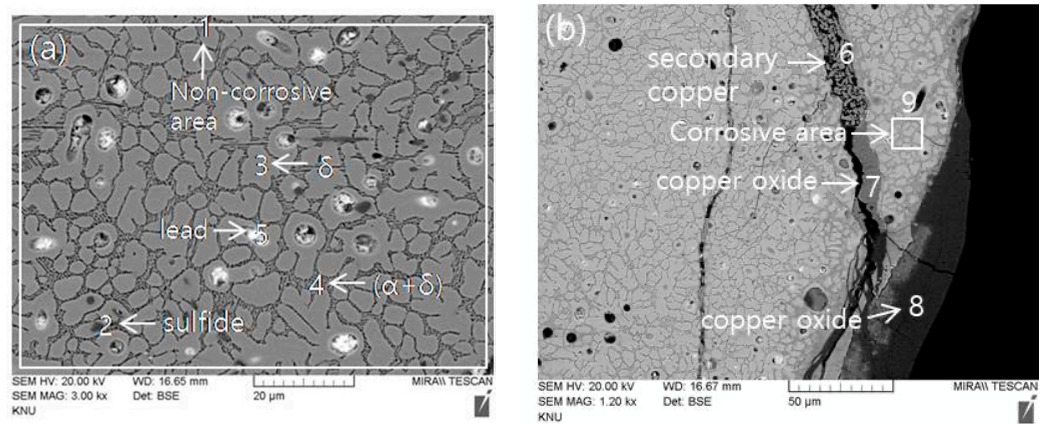
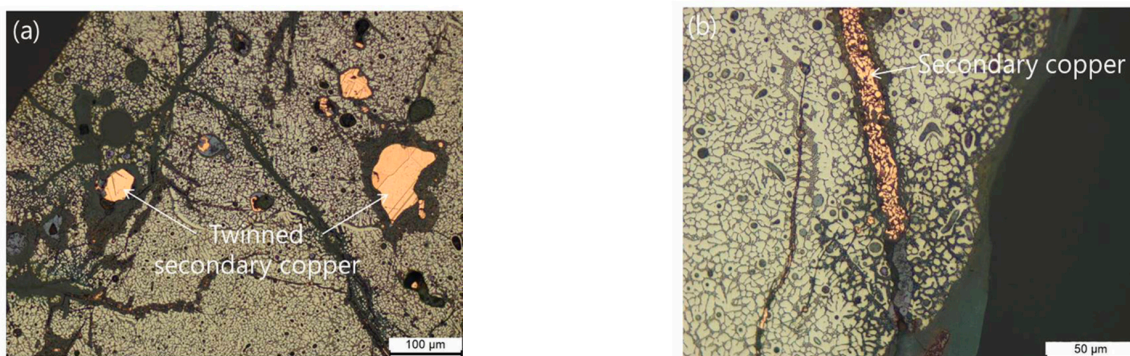


Figure 6. Ga-31 (No. 2) electron probe microanalyzer (EPMA) mapping image.

The microstructure consisted of  $\alpha + \delta$  eutectoid and  $\delta$  phases with sporadic sulfide and lead particles (Figure 7a). Its secondary copper likely formed as clumps in the corroded Pb particles or cracks, and twin crystals were observed in some cases (Figure 8a). Secondary copper with twin crystals is a product of the alloy's constituent components undergoing extended mineralization, production technique, and burial environment [14]. In addition, black corrosion products observed on the mirror's surface during excavation appeared because mineralized cassiterite formed on the surface.



**Figure 7.** (a) Ga-31 (No. 2) scanning electron microscope-energy dispersive spectrometer (SEM-EDS) images that show the original microstructure without corrosion and (b) secondary copper present in cracks formed from corrosion compounds.



**Figure 8.** Ga-31 (No. 2) optical micrograph images showing (a) twinned secondary copper and (b) secondary copper in corrosion.

In the secondary copper, Cu and O differed according to the degree of corrosion, and greater corrosion levels increased O and reduced Cu content. Because the Cu and O content standards between secondary copper and copper oxides remain unclear, determining secondary copper and copper oxide can be difficult. Here, a sample was observed under a metallurgical microscope. Pure secondary copper has an orange hue similar to metallic copper, while copper oxides have grey, cloudy hues. Despite losing its hue, copper oxide undergoing early stages of corrosion is nearly as pure as secondary copper. Thus, secondary copper and copper oxide were determined using EDS analysis and visually confirmed

using a metallurgical microscope. EDS positions 6 to 8, based on Cu and O content (6: metallic copper, 7: copper oxide undergoing corrosion, 8: copper oxide mineralized through corrosion), showed that metallic copper undergoing corrosion created cracks within the microstructure and exited to form corrosion compounds on the bronze artifact. (Figure 7b and Table 2).

**Table 2.** Ga-31 (No. 2) microstructure energy dispersive spectrometer (EDS) results.

No.	Position	Element (wt%)						
		O	S	Cu	Sn	Pb	Fe	Cl
2	1	0.37	—	68.24	27.90	3.48	—	—
	2	0.49	16.12	78.26	2.58	—	2.55	—
	3	—	—	68.29	31.71	—	—	—
	4	—	—	72.17	27.83	—	—	—
	5	5.67	—	6.98	—	87.35	—	—
	6	—	—	100.00	—	—	—	—
	7	4.33	—	90.07	4.79	0.34	—	0.47
	8	17.86	—	79.94	—	2.20	—	—
	9	3.87	—	55.67	35.28	5.18	—	—

### 3.3. Bronze Mirror Excavated from Pit Tomb Ga-35 (No. 3)

#### 3.3.1. Metal

The sample showed selective corrosion on the  $\alpha + \delta$  eutectoid phase along the boundaries and cracks as thick layers of red and green corrosion materials. According to the bronze artifact corrosion layer classification system, this mirror was classified under the type II corrosion category [9]. The microstructure consisted of  $\alpha + \delta$  eutectoid and  $\delta$  phases, with scattered sulfide and lead particles (Figure 9a and Table 3).

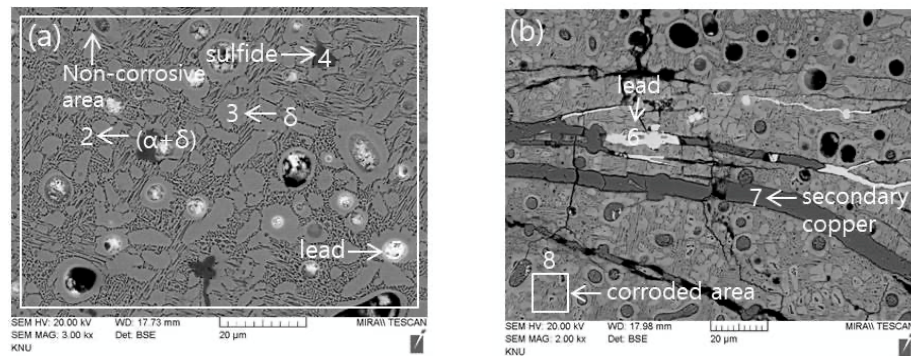


**Figure 9.** Ga-35 (No. 3) scanning electron microscope-energy dispersive spectrometer (SEM-EDS) images that show an uncorroded microstructure (a) and a line composed of secondary copper in the corroded microstructure (b).

**Table 3.** Ga-35 (No. 3) microstructure energy dispersive spectrometer (EDS) results.

No.	Position	Element (wt%)					
		O	S	Cu	Sn	Pb	Fe
3	1	1.34	0.15	64.87	29.10	4.55	—
	2	1.24	—	68.37	27.73	2.66	—
	3	—	—	66.51	33.49	—	—
	4	0.73	23.91	60.13	0.60	—	14.63
	5	7.13	—	8.50	1.61	82.76	—
	6	13.22	6.81	2.06	—	77.91	—
	7	5.12	—	94.88	—	—	—
	8	17.51	—	8.59	66.95	6.96	—

Because the bronze mirrors showed similar microstructures and distributions, they were most likely produced with the same techniques in a similar period. According to the ICP-AES analysis, a relatively small amount of Pb (0.85% to 1.10%) was detected, and all of them are ternary alloys of Cu-Sn-Pb (Table 4).

**Table 4.** Chemical composition of bronze mirrors obtained from the Sinpung site using inductively coupled plasma atomic emission spectroscopy (ICP-AES) analysis.

No.	Name	Composition (%)									
		Cu	Sn	Pb	As	Ag	Co	Fe	Ni	Sb	Zn
1	Ga-2	64.3	28.2	0.85	0.1684	0.0182	0.1204	0.0194	0.1555	0.0670	0.000273
2	Ga-31	63.9	28.3	1.10	0.1858	0.0292	0.1520	0.0745	0.1605	0.0867	0.000450
3	Ga-35	60.8	25.6	1.21	0.3567	0.0156	0.0410	0.0816	0.0791	0.1827	0.000941

In the Ga-35 (No. 3) bronze mirror, Pb and S appear to be present as lead sulfide, caused by the ore being added during the manufacturing process. Regarding the lead ore, previous studies on bronze production by-products excavated from the Wanju Sinpung ruins suggested that galena (PbS) obtained from southern Korean mines may have been used for smelting [15]. Sulfides were present in the bronze mirror's microstructures, but EDS detected only S or a combination of S and Fe. Secondary copper was found in clustered particles or lines, and twins were observed in some secondary copper (Figure 10).

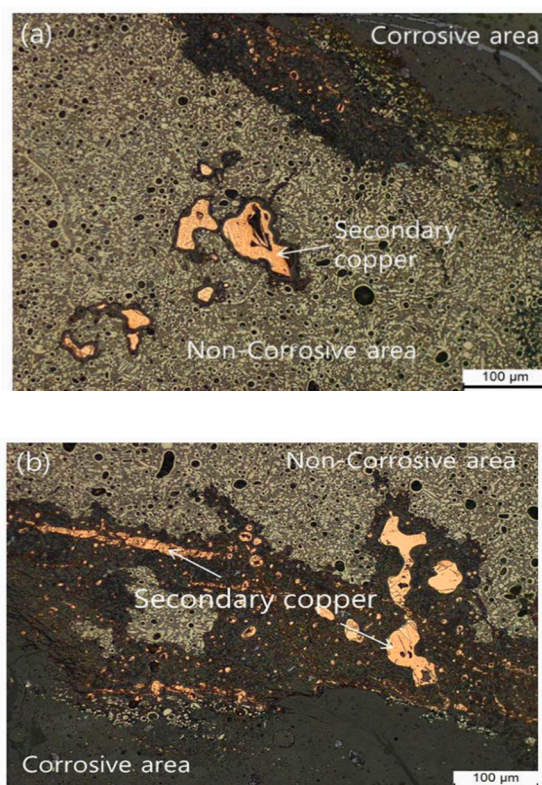


**Figure 10.** Ga-35 (No. 3) optical micrograph with secondary copper particles (a) and twinned secondary copper (b).

### 3.3.2. Patina

Enlarging the corrosion layers of the bronze mirror in DF photography revealed thick, localized layers of red and green corrosion products. According to the classification system proposed by Robbiola et al. [10], this falls under type II corrosion. Through micro-Raman spectroscopy, the dark green corrosion product (a) was determined as malachite

((Cu<sub>2</sub>CO<sub>3</sub>(OH)<sub>2</sub>), the red corrosion product (b) was cuprite (Cu<sub>2</sub>O), and the bright green corrosion product (c) was cassiterite (SnO<sub>2</sub>) (Figure 11a).

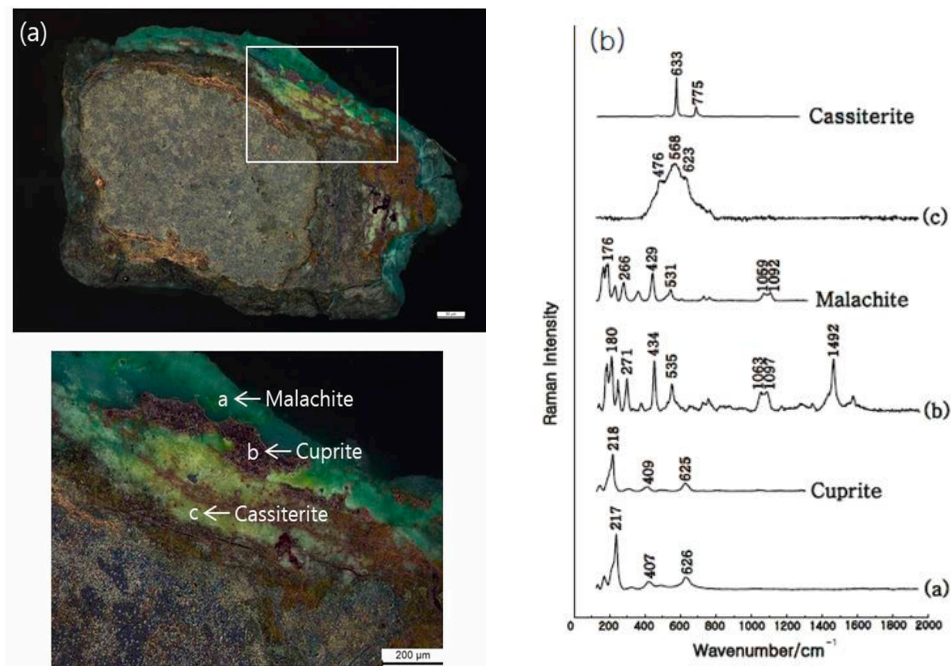


Figure 11. (a) Ga-35 (No. 3) corrosion layer darkfield (DF) images and (b) Raman spectrum.

Based on the EPMA mapping analysis results (Figure 12), corrosion layers with large amounts of Sn formed in the corroded microstructure because O and Sn content was remarkably high in the sections under the corrosion layer. From the EPMA line analysis, Cu and Sn exhibit inversely proportional correlations relative to their overall positions (Figure 13). In an external environment, anions such as CO<sub>3</sub><sup>2-</sup> and O<sup>2-</sup> move to the bronze alloy’s interior, while cations of metals such as Cu and Sn move outward and bond with each other to form and maintain a corrosion layer [16].

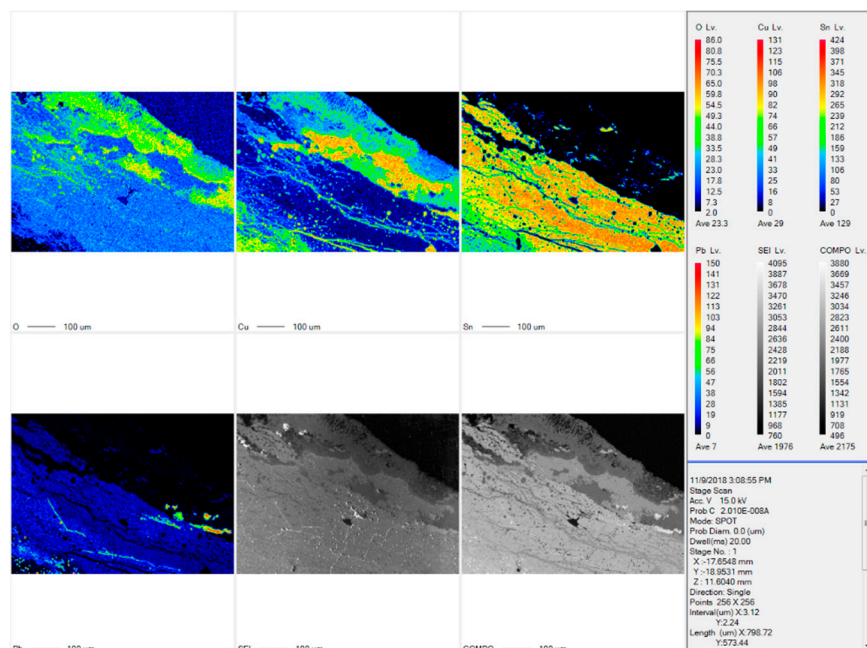


Figure 12. Ga-35 (No. 3) electron probe microanalyzer (EPMA) mapping image.

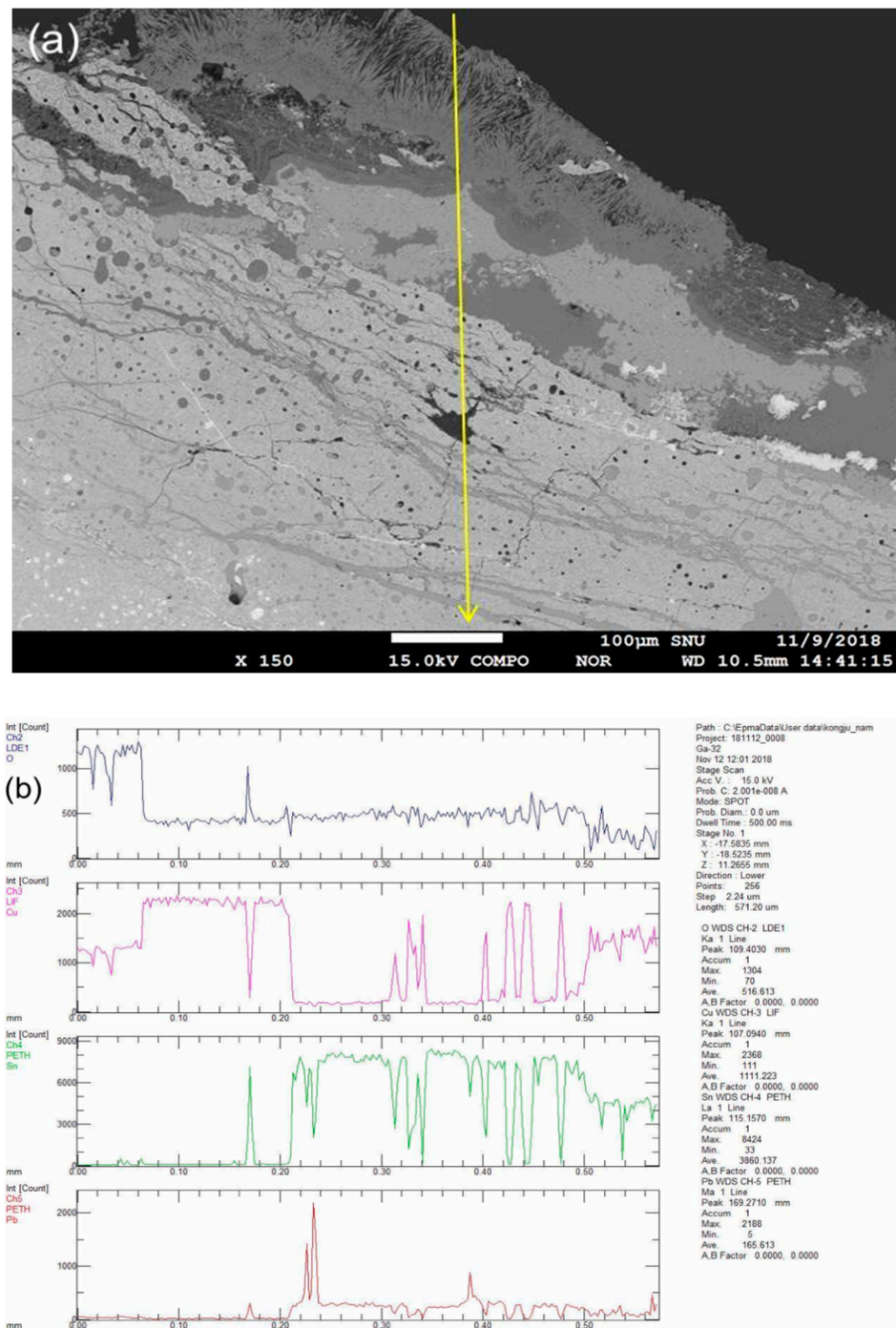


Figure 13. (a) Ga-35 (No. 3) electron probe microanalyzer (EPMA) image and (b) line analysis.

#### 4. Conclusions

This study analyzed the metallurgical and corrosion characteristics of Early Iron Age bronze mirrors excavated in the Sinpung site in Wanju. According to the ICP-AES results, the bronze mirrors were cast with a triple bronze Cu-Sn-Pb alloy (60% to 65% Cu, 25% to 28% Sn, and 0.85% to 1.21% Pb). Their metallic microstructures consisted of an  $\delta$  phase and an  $\alpha + \delta$  eutectoid phase, and there was no evidence of further treatment after casting. Lead sulfide was observed in the microstructure of the Ga-35 (No. 3) bronze mirror, suggesting that its lead content originated from lead ores used to produce the artifacts. Sulfides containing Fe from copper sulfide ore or Cu-Fe-S residual matte were also added to the bronze mirrors while being manufactured.

For corrosion characteristics, selective corrosion in the  $\alpha + \delta$  eutectoid phase was observed at the sample's surface, where selective corrosion in the  $\alpha$  phase was correlated with the oxidation environment. In contrast, selective corrosion in the  $\alpha + \delta$  eutectoid phase was correlated with a reducing burial environment [8]. According to Robbiola et al.'s classification system [9], Ga-2 and Ga-35 contained corrosion materials classified as type I corrosion. Meanwhile, nanocrystalline SnO<sub>2</sub> observed in bronze mirrors buried for long periods in soil was observed in type I and type II corrosion.

High-purity secondary copper in the artifacts was mainly located in cracks, holes left by Pb corrosion, and the corroded  $\alpha + \delta$  eutectoid phase. The secondary copper was classified according to Wang and Merkel's [8] proposal as it followed similar patterns. They distinguished the formation mechanism of secondary copper into two types: redeposition and destannification. In metallic copper formed through the former, Cu ions could not move freely and form metallic structures. In the samples, metallic copper was found in cracks, holes, and between cuprite formations formed through redeposition. In comparison, metallic copper formations found as pseudomorphs on the  $\alpha + \delta$  eutectoid phase formed through destannification because copper moved inward and replaced the existing metallic structures following Sn's selective corrosion. Thus, the secondary copper observed in holes left by corroded Pb particles and cracks on the excavated mirrors formed through redeposition. In contrast, the secondary copper formations observed on the  $\alpha + \delta$  eutectoid phase were created through destannification.

Various analytical techniques were used on bronze mirrors excavated from the Singung site to identify their production techniques and corrosion characteristics. Compared to other artifacts excavated from the site, weapons (swords) and tools (plows) contained Pb oxides, such as cerussite (PbCO<sub>3</sub>), anglesite (PbSO<sub>4</sub>), and litharge (PbO), as corrosion products, which were absent in bronze mirrors [17]. This contrast shows that the mirrors exhibited different corrosion characteristics caused by differences in alloy compositions or production techniques. The presence of malachite, which does not form in an underwater burial environment, indicated that corrosion characteristics could only be found in bronze mirrors excavated from the ground [18]. The corrosive properties of pure bronze artifacts also showed a heterogeneity that cannot be simulated in an artificial environment. Therefore, this study's results are of great importance for preserving artifacts and evaluating an artifact's authenticity. Moreover, future studies must develop a multifaceted analysis of various bronze artifacts and develop a comprehensive understanding of burial environments to establish long-term corrosion mechanisms in ancient bronze artifacts.

**Author Contributions:** Conceptualization, N.C.C.; methodology, I.K.H.; software, I.K.H.; validation, N.C.C.; formal analysis, M.K.J.; investigation, I.K.H.; resources, M.K.J.; data curation, M.K.J.; writing—original draft preparation, M.K.J.; writing—review and editing, I.K.H.; visualization, M.K.J.; supervision, N.C.C.; project administration, M.K.J.; funding acquisition, N.C.C. All authors have read and agreed to the published version of the manuscript.

**Funding:** This work was supported by the research grant of the Kongju National University in 2018.

**Institutional Review Board Statement:** Not applicable.

**Informed Consent Statement:** Not applicable.

**Data Availability Statement:** The data presented in this study are openly available in Mendeley Data at DOI: 10.17632/8h2k4j9xw6.1

**Conflicts of Interest:** The authors declare no conflict of interest.

## References

1. Scott, D.A. *Copper and Bronze in Art: Corrosion, Colorants, Conservation*; Getty Conservation Institute: Los Angeles, CA, USA, 2002.
2. Han, S.Y. An analysis of how the early iron age culture evolved, with a focus on the relics in Wanju Shinpung. *J. Honam Archaeol. Soc.* **2017**, *56*, 4–23. Available online: <https://scienceon.kisti.re.kr/srch/selectPORSrchArticle.do?cn=ART002239597> (accessed on 1 February 2021).

3. The Korean Christian Museum at Soongsil University. *Danyu Semunkyung: Comprehensive Research*; Soongsil University Korean Christian Museum: Seoul, Korea, 2009. Available online: <https://iss.ndl.go.jp/books/R100000096-I001868103-00?ar=4e1f&locale=ko> (accessed on 1 February 2021).
4. Honam Cultural Property Research Center. Shinpung Site, Wanju: Excavation Report Series 180. 2014. Available online: [http://www.kaah.kr/kcpia\\_book/sub/book\\_template.php?IncFile=200&code=13850](http://www.kaah.kr/kcpia_book/sub/book_template.php?IncFile=200&code=13850) (accessed on 3 December 2020).
5. Lafuente, B.; Downs, R.T.; Yang, H.; Stone, N. The power of databases: The RRUFF project. In *Highlights in Mineralogical Crystallography*; Armbruster, T., Danisi, R.M., Eds.; Walter de Gruyter GmbH: Berlin, Germany, 2015; pp. 1–29.
6. Chase, W.T. Chinese bronzes: Casting, finishing, patination and corrosion. In *Ancient & Historic Metals: Conservation and Scientific Research*; Scott, D.A., Podany, J., Considine, B.B., Eds.; Getty Conservation Institute: Los Angeles, CA, USA, 1995; pp. 85–119.
7. Lee, E.-W.; Kim, S.-J.; Han, W.-R.; Hwang, J.-J.; Han, M.-S. Morphology and characteristics of corrosion of archaeological bronzes. *MUNHWAJAE Korean J. Cult. Herit. Stud.* **2013**, *46*, 4–15. [[CrossRef](#)]
8. Wang, Q.; Merkel, J.F. Studies on the redeposition of copper in Jin bronzes from Tianma–Qucun, Shanxi, China. *Stud. Conserv.* **2001**, *46*, 242–250. [[CrossRef](#)]
9. Robbiola, L.; Blengino, J.M.; Fiaud, C. Morphology and mechanisms of formation of natural patinas on archaeological Cu-Sn alloys. *Corros. Sci.* **1998**, *44*, 2083–2111. [[CrossRef](#)]
10. Ospitali, F.; Chiavari, C.; Martini, C.; Bernardi, E.; Passarini, F.; Robbiola, L. The characterization of Sn-based corrosion products in ancient bronzes: A Raman approach. *J. Raman Spectrosc.* **2012**, *43*, 1596–1603. [[CrossRef](#)]
11. Abello, L.; Bochu, B.; Gaskov, A.; Koudryavtseva, S.; Lucazeau, G.; Roumyantseva, M. Structural characterization of nanocrystalline SnO<sub>2</sub> by X-ray and Raman spectroscopy. *J. Solid State Chem.* **1998**, *135*, 78–85. [[CrossRef](#)]
12. Dieguéz, A.; Romano-Rodriguez, A.; Vilà, A.; Morante, J.R. The complete Raman spectrum of nanometric SnO<sub>2</sub> particles. *J. Appl. Phys.* **2001**, *90*, 1550–1557. [[CrossRef](#)]
13. Pagnier, T.; Boulova, M.; Sergent, N.; Bouvier, P.; Lucazeau, G. Nanopowders and nanostructured oxides: Phase transitions and surface reactivity. *J. Raman Spectrosc.* **2007**, *38*, 756–761. [[CrossRef](#)]
14. Jang, M.K. Study on Manufacturing Technique and Corrosion Characteristics of Bronze Mirrors in Early Iron Age Excavated from Sinpung Site in Wanju, Korea. Master’s Thesis, Kongju National University, Gongju, Korea, 2020. Available online: [http://www.riss.kr/search/detail/DetailView.do?p\\_mat\\_type=be54d9b8bc7cdb09&control\\_no=ce509e3ca95f4055ffe0bdc3ef48d419&outLink=N](http://www.riss.kr/search/detail/DetailView.do?p_mat_type=be54d9b8bc7cdb09&control_no=ce509e3ca95f4055ffe0bdc3ef48d419&outLink=N) (accessed on 1 February 2021).
15. Choi, N.Y. A Metallurgical Study on the By-Products of the Bronze Production in the Goryeo Dynasty as Excavated from Sinpung Site in Wanju, Jeollabuk-do, Republic of Korea. Master’s Thesis, Kongju National University, Gongju, Korea, 2017. Available online: [http://www.riss.kr/search/detail/DetailView.do?p\\_mat\\_type=be54d9b8bc7cdb09&control\\_no=161152f33063c160ffe0bdc3ef48d419&outLink=N](http://www.riss.kr/search/detail/DetailView.do?p_mat_type=be54d9b8bc7cdb09&control_no=161152f33063c160ffe0bdc3ef48d419&outLink=N) (accessed on 1 February 2021).
16. Trentelman, K.; Stodulski, L.; Lints, R.; Kim, C. A comparative study of the composition and corrosion of branches from Eastern Han dynasty money trees. *Stud. Conserv.* **1999**, *44*, 170–183. [[CrossRef](#)]
17. Jang, M.K.; Cho, N.C. A study on the corrosion and microstructure characteristics of Early Iron Age bronze swords excavated from Sinpung Site in Wanju, Jeollabuk-Do, Republic of Korea. *Korean J. Met. Mater.* **2020**, *58*, 472–479. [[CrossRef](#)]
18. Kim, K.B. Anaerobic Corrosion Properties of Copper Alloy Objects Underwater. Master’s Thesis, Korea National University of Cultural Heritage, Boyeo, Korea, 2017. Available online: [https://academic.naver.com/article.naver?doc\\_id=443879362](https://academic.naver.com/article.naver?doc_id=443879362) (accessed on 1 February 2021).